Effective Use of the Linear Fine Mesh Rebalance for the DSA of S_N Transport Equation with Tetrahedral Meshes

Habib Muhammad, Ser Gi Hong*

Kyung Hee University, Department of Nuclear Engineering
Deogyeong-daero, GiHeung-gu, Yongin, Gyeonggi-do, 446-701 Korea
**sergihong@khu.ac.kr*

INTRODUCTION

This paper presents a diffusion synthetic acceleration (DSA) technique coupled with the linear fine mesh rebalance (FMR) method for the S_N transport equation discretized with the linear discontinuous expansion method with subcell balance (LDEM-SCB). The LDEM-SCB scheme solves the transport equation with discrete ordinates method by using the subcell balances and discontinuous linear expansion of flux [1]. The DSA equations are derived by consistently discretizing the continuous diffusion transport equation with LDEM-SCB(1) in our previous work [2]. Our previous work showed that the DSA is very efficient in reducing the number of transport sweeps but the method to effectively solve the diffusion equation was not suggested. In this paper, we suggest the use of a linear FMR method to effectively solve the discretized diffusion equations. In particular, the FMR equations are solved with the conjugate gradient (CG) method. The effectiveness of the DSA method is tested for a homogeneous 3D problem having varying total cross sections.

DERIVATION OF DSA EQUATIONS

It has been well known that the iterative solutions of the transport equations converge very slowly in high scattering dominant regions having optically thick size. Therefore, the works to develop acceleration methods to speed up the convergence have been always very active research area in nuclear engineering [3]. One of them, the DSA is a very powerful method to accelerate the convergence of the source iteration [4-6]. The development of an efficient DSA scheme is a critical issue in the numerical methods for solving the transport equation for the complicated geometries [6-9].

The second author devised the LDEM-SCB(1) method to solve the multigroup S_N transport equation with the tetrahedral meshes. This method expands the neutron flux with linear discontinuous functions and the coupling equations for the unknown fluxes are derived using the subcell balance equations [1]. This method uses the subcell division given in Fig. 1. The DSA equation for LDEM-SCB(1) is derived by discretizing the following continuous diffusion equation in a consistent manner with the LDEM-SCB(1):

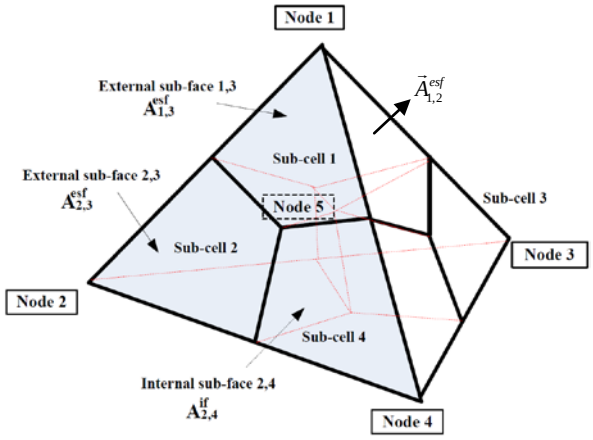

Fig. 1. Subcell division for LDEM-SCB(1)

$$\nabla \cdot \vec{F}^{(\ell+1)}(\vec{r}) + \sigma_a f^{(\ell+1)}(\vec{r}) = q^{(\ell+1/2)}(\vec{r}) \,, \tag{1}$$

$$\frac{1}{3}\nabla f^{(\ell+1)}(\vec{r}) + \sigma_t \vec{F}^{(\ell+1)}(\vec{r}) = 0 \,, \tag{2}$$

where the source q, the scalar flux correction *f*, and the current vector correction $\vec{F}$ are given by

$$q^{(\ell+1/2)}(\vec{r}) = \sigma_s\left(\phi^{(\ell+1/2)}(\vec{r}) - \phi^{(\ell)}(\vec{r})\right) \,,$$

$$f^{(\ell+1)}(\vec{r}) = \phi^{(\ell+1)}(\vec{r}) - \phi^{(\ell+1/2)}(\vec{r}) \,, \tag{3}$$

$$\vec{F}_1^{(\ell+1)}(\vec{r}) = \vec{J}_1^{(\ell+1)}(\vec{r}) - \vec{J}_1^{(\ell+1/2)}(\vec{r}) \,.$$

In Eq. (3), the fluxes having $(\ell+1/2)$ index represent the results of transport sweep while the ones having $(\ell+1)$ and (ℓ) represent the flux obtained with the DSA and the flux before the transport sweeping, respectively. Next, we discretize the continuous diffusion equation (i.e., Eqs. (1) and (2)) in a consistent manner with LDEM-SCB(1). First, the subcell balance equations are obtained by integrating Eq. (1) over a subcell. For example, the balance equation over the first subcell of a tetrahedron cell '*k*' is given by

$$\int_{V_{sc1}^k} \nabla \cdot \vec{F}^{k,(\ell+1)} dV + \int_{V_{sc1}^k} \sigma_a^k f^{k,(\ell+1)} dV = \int_{V_{sc1}^k} q^{k,(\ell+1/2)} dV. \quad (4)$$

Applying the Green's theorem to Eq. (4) after dropping the iteration index for simplicity gives

$$\int_{A_{sc1}} dA \vec{F}^k \cdot \hat{n} + \sigma_a^k \bar{f}_{sc1}^k V_{sc1}^k = \bar{q}_{sc1}^k V_{sc1}^k, \quad (5)$$

where $\bar{f}_{sc1}^k$ and $\bar{q}_{sc1}^k$ are the average values of the scalar flux correction and the source, respectively, over the first subcell of the present cell '*k*' and V_{sc1}^k is the volume of the first subcell. Then, the surface integral of current vector correction $\vec{F}$ in Eq. (5) is splitted into the outgoing and the incoming partial current corrections over the external faces and the internal interfaces of the first subcell. For example, this integral over the external subface $\vec{A}_{1,2}^{esf}$ is given by

$$\vec{F}_{1,2}^{esf} \cdot \vec{A}_{1,2}^{esf} = \frac{1}{3} \left| \vec{A}_2^k \right| \left(F_{1,2}^{+,k} - F_{\alpha,\beta}^{+,k'(1,2)} \right), \quad (6)$$

where $\vec{A}_2^k$ is the external surface area opposite to the node 2 and $\vec{A}_{1,2}^{esf}$ represents the subface area which is a part of $\vec{A}_2^k$ and has the node 1 as its point i.e. $\vec{A}_{1,2}^{esf} = \vec{A}_2^k / 3$ (see Fig. 1) and the index $k'(1,2)$ represents the neighboring cell of the present cell '*k*' through the subface $\vec{A}_{1,2}^{esf}$. In Eq. (6), 'α' and 'β' are the local node indices of the neighbouring cell $k'(1,2)$ and they identify $\vec{A}_{1,2}^{esf}$. Then, the partial current corrections are represented in terms of the scalar flux corrections in their cells. The derivation of this representation requires quite lengthy equations, so we omitted them. The substitution of these representations of the surface integral terms into Eq. (5) leads to the following DSA equation for the first subcell:

$$\begin{aligned}
&\left\{ 22\left(\left|\vec{A}_2^k\right| + \left|\vec{A}_3^k\right| + \left|\vec{A}_4^k\right| \right) + \tilde{D}_k \left(\vec{A}_1^k \cdot \vec{A}_1^k \right) + 225\sigma_a^k V_{sc1}^k \right\} f_1^{k,(p+1/2)} \\
&+ \left\{ 7\left(\left|\vec{A}_3^k\right| + \left|\vec{A}_4^k\right| \right) + \tilde{D}_k \left(\vec{A}_1^k \cdot \vec{A}_2^k \right) + 69\sigma_a^k V_{sc1}^k \right\} f_2^{k,(p+1/2)} \\
&+ \left\{ 7\left(\left|\vec{A}_2^k\right| + \left|\vec{A}_4^k\right| \right) + \tilde{D}_k \left(\vec{A}_1^k \cdot \vec{A}_3^k \right) + 69\sigma_a^k V_{sc1}^k \right\} f_3^{k,(p+1/2)} \\
&+ \left\{ 7\left(\left|\vec{A}_2^k\right| + \left|\vec{A}_3^k\right| \right) + \tilde{D}_k \left(\vec{A}_1^k \cdot \vec{A}_4^k \right) + 69\sigma_a^k V_{sc1}^k \right\} f_4^{k,(p+1/2)} \\
&= V_{sc1}^k \left\{ 225 q_1^k + 69\left(q_2^k + q_3^k + q_4^k \right) \right\} + \sum_{j=2}^{4} \Theta_j,
\end{aligned} \quad (7)$$

where the term Θ_j is defined by

$$\begin{aligned}
\Theta_j &= \left|\vec{A}_j^k\right| \left\{ 22 f_\alpha^{k'(j),(p')} + 7\left(f_\beta^{k'(j),(p')} + f_\delta^{k'(j),(p')} \right) \right\} \\
&- \tilde{D}_{k'(j)} \left\{ \sum_{j'=1}^{4} \left(\vec{A}_j^k \cdot \vec{A}_{j'}^{k'(j)} \right) f_{j'}^{k'(j),(p')} \right\}.
\end{aligned} \quad (8)$$

In Eq. (7), f_i^k represents the scalar flux correction at the i^{th} node of the present cell '*k*', $\tilde{D}_k = 24 D_k / V_k$, and (p) represents the iteration index for DSA equation. In Eq. (8), the cell index $k'(j)$ represents the neighboring cell opposite to the j^{th} face of the present cell '*k*'. Also, it should be noted that the iteration index (p') for the DSA depends on the cells. That's to say, the iteration index (p') becomes $(p+1/2)$ if the cell $k'(j)$ has already been swept and otherwise it becomes (p).

The remaining DSA equations for the other three subcells can be derived in the same manners. Actually, the discretized diffusion equations represent a discontinuous discretization (not continuous one) of the diffusion equation and we solve them using a Gauss Seidel-like sweeping iteration, which is represented by the iteration index (p) in Eq. (7).

DERIVATION OF FMR EQUATION

In this work, we suggest a linear FMR method to accelerate the Gauss Seidel-like iteration for the DSA equation (i.e., Eq. (7)). The derivation of the FMR equation starts with the balance equation which is just obtained by integrating Eq. (1) over a tetrahedral cell '*k*'. The resulting equation is given by

$$\begin{aligned}
&\sum_{j=1}^{4} \left[\sum_{\substack{j'=1 \\ j' \neq j}}^{4} \left|\vec{A}_{j'}^k\right| + 3\sigma_a^k V_k + \frac{\tilde{D}_k}{12} \sum_{j'=1}^{4} \left(\vec{A}_j^k \cdot \vec{A}_{j'}^k \right) \right] f_j^{k,(p+1)} \\
&- \sum_{j=1}^{4} \xi_j = 12 \bar{q}_k V_k,
\end{aligned} \quad (9)$$

where the term ξ_j is defined by

$$\begin{aligned}
\xi_j &= \left|\vec{A}_j^k\right| \left(f_\alpha^{k'(j),(p+1)} + f_\beta^{k'(j),(p+1)} + f_\delta^{k'(j),(p+1)} \right) \\
&- \frac{\tilde{D}_{k'(j)}}{12} \sum_{j'=1}^{4} \left\{ \left(\vec{A}_j^k \cdot \vec{A}_{j'}^{k'(j)} \right) f_{j'}^{k'(j),(p+1)} \right\}.
\end{aligned} \quad (10)$$

For the linear FMR method, we define the additive rebalance factor for the scalar flux correction as follows:

$$f_j^{k,(p+1)} = f_j^{k,(p+1/2)} + \gamma_k^{(p+1)}. \quad (11)$$

Substitution of Eq. (11) into Eq. (9) gives the following final linear rebalance equation over the cell '*k*':

$$3\left\{\sum_{j=1}^{4}\left|\vec{A}_j^k\right|+4\sigma_a^k V_k\right\}\gamma_k^{(p+1)}-3\sum_{j=1}^{4}\left(\left|\vec{A}_j^k\right|\gamma_{k'(j)}^{(p+1)}\right) \quad (12)$$
$$=12\bar{q}_k V_k+\sum_{j=1}^{4}\xi_{1j}-\sum_{j=1}^{4}\xi_{2j},$$

where $\gamma_{k'(j)}^{(p+1)}$ is the FMR factor for the neighboring cell $k'(j)$. The terms ξ_{1j} and ξ_{2j} are defined by

$$\xi_{1j}=\left|\vec{A}_j^k\right|\left(f_\alpha^{k'(j),(p+1/2)}+f_\beta^{k'(j),(p+1/2)}+f_\delta^{k'(j),(p+1/2)}\right) \quad (13)$$
$$-\frac{\tilde{D}_{k'(j)}}{12}\sum_{j'=1}^{4}\left\{\left(\vec{A}_j^k\cdot\vec{A}_{j'}^{k'(j)}\right)f_{j'}^{k'(j),(p+1/2)}\right\},$$

and

$$\xi_{2j}=\left(3\sigma_a^k V_k+\sum_{\substack{j'=1\\ j'\neq j}}^{4}\left|\vec{A}_{j'}^k\right|+\frac{\tilde{D}_k}{12}\sum_{j'=1}^{4}\left(\vec{A}_j^k\cdot\vec{A}_{j'}^k\right)\right)f_j^{k,(p+1/2)}. \quad (14)$$

These rebalance equations constitute a system of linear equations whose matrix is symmetric positive definite (SPD) and we applied the conjugate gradient (CG) method for solving them.

RESULTS

In this section, our DSA method with the linear FMR method is tested with a one group homogeneous problem having a source of 10 neutrons/cm^{3}sec and it is comprised of 30×30×30 grid of unit cubes. The side length of each unit cube is 1.0 cm. Each unit cube is divided into six tetrahedrons. The reflective boundary conditions (BCs) are applied to the -x, -y, and -z external faces while the vacuum BCs are applied to all other external faces. The scattering ratio is fixed to 0.9999 but the total cross section is varied. The pointwise convergence criteria for the source iteration of the transport, the DSA and the FMR equations are 1.0×10^{-8}, 1.0×10^{-3} and 1.0×10^{-2}, respectively.

We used two azimuthal angles and two polar angles per octant with the Chebyshev-Legendre quadrature for all the problems. We consider five different cases having different total cross sections with a fixed scattering ratio of 0.9999; the results are summarized in Table I. These results show that the DSA is very effective in accelerating the solution of the transport equation in terms of the number of transport sweeps and the computing time. The speedup factor is the ratio of time to solve transport equation with and without DSA. The speedup ranges from 9.6 to 25.7 times. The speedup increases as the total cross section increases (i.e. as the problem size increases in mean free path) because the dependency of the DSA performance on the total cross section is weaker than that of source iteration. From our experience of the FMR, it is found that the application of the FMR without the CG algorithm to the DSA appears to be ineffective and even fails for some problems because of its very large number of sweeps and instability.

Table I. Comparison of DSA performances for various total cross sections

Test Case	Total Cross Section (cm^{-1})	SI without DSA		SI with DSA (with FMR)		Speedup
		Number of Transport Sweeps	Time (hrs)	Number of Transport Sweeps	Time (hrs)	
I	1.0	4698	5.033	15	0.523	9.6
II	1.5	9367	9.167	16	0.542	16.9
III	2.0	14936	14.47	15	0.697	20.8
IV	2.5	20982	20.81	15	0.77	25.0
V	3.0	27161	26.93	15	1.049	25.7

Fig. 2 shows the average numbers of FMR (CG) sweeps over each DSA sweep for all the test cases. It shows that the average number of FMR (CG) sweeps after each DSA iteration slightly increases as the total cross section increases but this increase is small in the last three cases. Fig. 2 also shows that the CG method is needed to be further improved to reduce the number of CG iterations. In the future, we will consider some preconditioning for CG method.

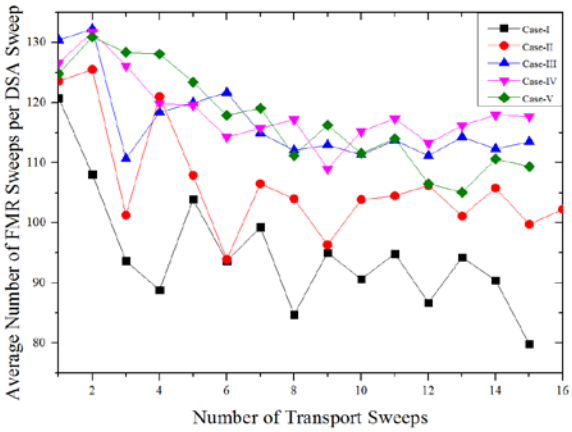

Fig. 2. Comparison of FMR (CG) sweeps for test cases over the DSA sweeps

Table II compares the numbers of the DSA sweeps for each transport sweep with and without the FMR application to DSA. From this table, it is considered that the FMR is very effective both in reducing the number of the DSA sweeps and the computing time. The speedup factor in this case shows that the DSA acceleration with the FMR (CG) method is much more effective than the DSA without the FMR method. In particular, the numbers of DSA sweeps are drastically reduced with the FMR. At present, we did not consider any preconditioning for the CG method. The numerical estimates of spectral radius are also given in the Table II and they slightly increase as the total cross section increases but they are less than 0.38.

Table II. Comparison of DSA sweeps count with and without FMR coupled with DSA

Transport Sweeping Number	Case I		Case II		Case III		Case IV		Case V	
	Number of DSA Sweeps	Number of DSA Sweeps with FMR	Number of DSA Sweeps	Number of DSA Sweeps with FMR	Number of DSA Sweeps	Number of DSA Sweeps with FMR	Number of DSA Sweeps	Number of DSA Sweeps with FMR	Number of DSA Sweeps	Number of DSA Sweeps with FMR
1	766	31	827	17	875	24	897	24	903	29
2	3660	52	3785	38	3165	51	2443	67	2144	81
3	11280	26	15446	14	19888	15	2291	20	18350	28
4	918	41	2516	26	8596	30	10094	36	15197	58
5	1944	26	1905	13	17515	35	24415	55	24176	67
6	9893	26	16591	25	2651	38	9451	39	12154	51
7	1578	31	3918	27	15279	53	22103	36	20724	43
8	452	27	547	24	12870	32	21342	39	14209	45
9	10145	25	11582	25	12768	48	18191	40	19922	45
10	2710	23	10869	22	14445	32	15808	39	18661	44
11	412	24	12800	26	13631	49	13934	42	14179	51
12	9985	26	10960	25	17281	33	15085	38	19504	50
13	2477	29	11027	23	11225	49	17350	46	18841	57
14	2012	32	9215	24	13728	38	13505	46	20927	56
15	3728	35	7593	21	13551	41	16646	45	16783	58
16	-	-	8529	23	-	-	-	-	-	-
Time (hrs)	2.783	0.523	6.347	0.542	7.7803	0.697	9.8544	0.77	10.4086	1.049
Spectral radius	0.2927		0.2988		0.3348		0.3359		0.3732	
Speedup	5.3		11.7		11.2		12.8		9.9	

SUMMARY AND CONCLUSION

In this work, a linear fine mesh rebalance (FMR) scheme is devised and applied to the discontinuous diffusion discretization for the DSA of LDEM-SCB(1) in order to reduce the computing time. In particular, the linear FMR equations are solved using CG method. From the numerical test, it is concluded that the DSA method coupled with linear FMR (CG) is very effective both in reducing the number of transport sweeps and the computing time. Although, the CG method is found to be very efficient in solving the FMR equations and improving the overall efficiency of the DSA, there are still possibilities to improve the CG algorithm by using a preconditioning. In future work, we aim to apply a suitable preconditioning to the CG algorithm to further improve the DSA scheme.

REFERENCES

1. S. G. HONG, "Two Subcell Balance Methods for Solving the Multigroup Discrete Ordinates Transport Equation with Tetrahedral Meshes," *Nucl. Sci. Eng.*, **173**, 101-117 (2013).

2. H. MUHAMMAD, S. G. HONG, "Diffusion Synthetic Acceleration (DSA) for the Linear Discontinuous Expansion Method with Subcell Balance (LDEM-SCB)," *Trans. Kor. Nucl. Soc.*, Jeju, Korea, 16-18 May, 2018.

3. M. L. ADAMS, E. W. LARSEN, "Fast Iterative Methods for Discrete Ordinates Particle Transport Calculations," *Prog. Nucl. Eng.*, **40**, 3-159, (2002).

4. M. L. ADAMS, T. A. WAREING, "Diffusion Synthetic Acceleration Given Anisotropic, General Quadratures, and Multidimensions," *Nucl. Sci. Eng*., **68**, 203 (1993).

5. M. L. ADAMS, W. R. MARTIN, "Diffusion Synthetic Acceleration of Discontinuous Finite Element Transport Iterations," *Nucl. Sci. Eng*., **111**, 145-167 (1992).

6. J. S. WARSA, T. A. WAREING, J. E. MOREL, "Fully Consistent Diffusion Synthetic Acceleration of Linear Discontinuous S_N Transport Discretizations on Unstructured Tetrahedral Meshes," *Nucl. Sci. Eng*., **141**, 236-251 (July 2002).

7. T. A. WAREING, J. M. MCGHEE, J. E. MOREL, S. D. PAUTZ, "Discontinuous Finite Element S_N Methods on Three-Dimensional Unstructured Grids," *Nucl. Sci. Eng*., **138**, 256-268 (2001).

8. J. S. WARSA, "A Continuous Finite Element-Based Disconitnuous Finite Element Method for S_N Transport," *Nucl. Sci. Eng*., **160**, 385-400 (2008)

9. J. E. MOREL, J. S. WARSA, "An S_N Spatial Discretization Scheme for Tetrahedral Meshes," *Nucl. Sci. Eng*., **151**, 157-166 (2005).